Available online at www.sciencedirect.com
ScienceDirect
Geochimica et Cosmochimica Acta 71 (2007) 6002–6018
Geochimica et Cosmochimica Acta
www.elsevier.com/locate/gca

Structural control on bulk melt properties: Single and double quantum ^{29}Si NMR spectroscopy on alkali-silicate glasses

Wim J. Malfait [a,*], Werner E. Halter [a], Yann Morizet [a,1], Beat H. Meier [b], Rene Verel [b]

[a] *Institute for Isotope Geochemistry and Mineral Resources, ETH Zurich, Clausiusstrasse 25, CH-8092 Zürich, Switzerland*
[b] *Laboratory for Physical Chemistry, ETH Zurich, Wolfgang-Pauli-Strasse 10, CH-8093 Zürich, Switzerland*

Received 27 November 2006; accepted in revised form 12 September 2007; available online 26 September 2007

Abstract

The structure of 21 binary potassium, rubidium and cesium silicate glasses (in the range 15–50 mol% alkali oxide) was analyzed by ^{29}Si single quantum and double quantum MAS NMR spectroscopy. Their glass transition temperatures (T_g) were measured by calorimetry. The chemical shifts and the relative abundance of Q^n species correlate with the cationic field strength (Z/r) of the network modifier. A correlation is observed between T_g and the inverse of the entropy of mixing of the different Q^n species, which is explained in the framework of the Adam–Gibbs relaxation theory. At high alkali content, up to 44% of the SiO_4 tetrahedra are part of three-membered rings. At a given alkali content, the abundance of these rings increases with increasing cation size. The abundance of three-membered rings in K-silicate melts correlates with a temperature and a non-linear composition dependence of the heat capacity. It is also a possible cause for the anomalous volumetric behavior of potassium silicate glasses.

1. INTRODUCTION

The behavior of magmas in the Earth's crust is mainly controlled by the physical and thermodynamic properties of the melt phase. Thus, a detailed understanding of magmatic processes has to build on an accurate quantification of these properties (e.g. viscosity and heat capacity) at various conditions. In most cases, these properties are not a simple function of the chemical composition, temperature and pressure. Indeed, it appears from spectroscopic investigations that bulk properties depend on the short to medium range structure of the melts (e.g. Stebbins et al., 1995; Mysen and Richet, 2005).

The structure of silicate melts consists of a three-dimensional network of SiO_4 tetrahedra linked by bridging oxygen atoms (BO). Addition of network-modifying cation oxides breaks up this network by generating non-bridging oxygen atoms (NBO). Therefore, the structure of silicate glasses and melts can be described through the abundance of Q^n species, where n is the number of bridging oxygen atoms per SiO_4 tetrahedron, and the three-dimensional arrangement of the tetrahedra, e.g. the ring size distribution. The abundance of Q^n species is controlled by the following speciation reactions:

$$2Q^n = Q^{n-1} + Q^{n+1} \quad (n = 3, 2, 1) \tag{1}$$

with the following equilibrium constants K_n.

$$K_n = [Q^{n-1}] \cdot [Q^{n+1}]/[Q^n]^2 \tag{2}$$

In Eq. (2), the assumption was made that the activity coefficients cancel out.

The quantification of the Q^n speciation is not possible in natural composition silicate melts and glasses because the infrared, Raman and NMR spectra are too complex to be deconvoluted. To quantify the effect of temperature and composition on the speciation, binary alkali-silicate glasses

* Corresponding author. Fax: +41 44 632 1827.
E-mail address: malfait@erdw.ethz.ch (W.J. Malfait).
[1] Present address: Laboratoire de Planétologie et Géodynamique, Université de Nantes, 2 rue de la Houssinière, B.P. 92208, 44322 Nantes Cedex 3, France.

0016-7037/$ - see front matter © 2007 Elsevier Ltd. All rights reserved.
doi:10.1016/j.gca.2007.09.011

and melts, and the sodium silicate system in particular, have been studied extensively by various spectroscopic methods (e.g. nuclear magnetic resonance (NMR), Raman, infrared and X-ray absorption spectroscopy). Among those, ^{29}Si Magic Angle Spinning (MAS) NMR spectroscopy has provided the most accurate information on the Q^n speciation in glasses (e.g. Grimmer et al., 1984; Dupree et al., 1986; Stebbins, 1987; Emerson et al., 1989; Maekawa et al., 1991). More recently, ^{29}Si double quantum (DQ) MAS NMR spectroscopy has been successfully applied to study the connectivity between the different Q^n species, either through the dipolar coupling (e.g. Glock et al., 1998; Olivier et al., 1998, 2001) or through the J coupling (e.g. Fyfe et al., 1990).

Sodium silicate glasses have often been used as a model for other alkali and alkaline earth silicate glasses. There are significant differences, however, in the spectra of glasses with different network-modifying cations. For instance, Maekawa et al. (1991) observed an additional peak in the spectrum of K-silicate glasses and interpreted it as an additional Q^2 peak. This is in contrast to NMR spectra of Li- and Na-silicate glasses, where each Q^n species corresponds to just one peak. They tentatively assigned this additional peak to a specific type of Q^2, which is present in a ring configuration. This peak will be called $Q^{2'}$ for the remainder of this paper. This additional peak is also present in the spectra of Rb- and Cs-silicate glasses (Dupree et al., 1984); although it was assigned to Q^1 in the latter study.

Apart from the differences in the NMR spectra, there are also distinct differences in the physical properties of melts with different network-modifying cations. For example, in contrast to Li-, Na- and alkaline earth silicate melts, the heat capacity of K-silicate melts is temperature dependent and shows a non-linear compositional dependence (Richet and Bottinga, 1985). Also, Bockris et al. (1956) and Tomlinson et al. (1958) observed an anomalous volumetric behavior for K-silicate glasses compared to Li- and Na-silicate glasses and concluded that the accommodation of the large potassium cations has to be accompanied by a structural rearrangement.

The objective of this study is to determine if there is a link between the anomalous physical properties and the distinct spectroscopic features of potassium silicate glasses. We have used ^{29}Si NMR spectroscopy to quantify the speciation and to investigate the medium range order of K-, Rb- and Cs-silicate glasses. With these results, we can rationalize the temperature and compositional dependence of bulk properties through changes in the melt structure.

2. SAMPLES

Fourteen K-silicate glasses were prepared in the range 15–50 mol% K_2O. Additionally, three K-silicate glasses (42, 46 and 50 mol% K_2O) were prepared from ^{29}Si enriched SiO_2 (96.74% ^{29}Si, Isoflex) for the SQ/DQ correlation NMR experiments. Rb- and Cs-silicate glasses at the disilicate (33 mol% alkali oxide) and metasilicate (50 mol% alkali oxide) composition were also prepared. The glasses were prepared by mixing known amounts of reagent grade SiO_2 and M_2CO_3 (M = K, Rb, Cs), 0.1 wt% of Fe_2O_3 was added to the samples to reduce the T_1 relaxation time. The mixtures were melted three times in Pt crucibles for one hour at 100 K above their respective liquidus temperatures. This was reduced to three times twenty minutes for the most alkali rich samples to avoid unnecessary alkali volatization. Two intermediate crushings under ethanol were performed to ensure sample homogeneity. The glasses were quenched by dipping the bottom of the crucible in water (quench rate of 200–500 K/s). Since most of the glasses are very hygroscopic, all subsequent handling (e.g. sample crushing, filling of the NMR rotors) was done in a glove-bag under an argon atmosphere. The samples were stored as $\sim$0.5 cm^3 pieces in tightly screwed, argon filled, glass vials and crushed to $\sim$0.1–1 mm^3 pieces immediately prior to the filling of the NMR rotors. No changes in the NMR spectra were observed between samples that were measured 2 days after synthesis and samples that were stored for over a year prior to the analysis.

3. ANALYTICAL TECHNIQUES

3.1. Chemical analysis

The most silica rich sample was analyzed with a JEOL JXA-8200 electron probe micro analyzer (EPMA). The hygroscopic nature of the more alkali rich samples prevented the necessary sample preparation (polishing and coating) for microprobe analysis and/or the unstable nature of the glasses under the electron beam (Gedeon et al., 2000) rendered an accurate microprobe analysis impossible. Therefore, the composition of the K-silicate glasses was analyzed with an Axios XRF spectrometer (PANanalytical). The Rb- and Cs-silicate glasses could not be analyzed by XRF since no suitable standards were available for the unusually high Rb and Cs contents. The samples enriched in ^{29}Si were not analyzed due to the high cost of the sample.

Despite having been handled exclusively under an Argon atmosphere, a minimal contamination with water cannot be avoided because of the extreme hygroscopicity of the K_2O rich samples. The water content of the most hygroscopic sample (50 mol% K_2O) was quantified by proton NMR. The proton spectra were acquired on a Varian Infinity spectrometer equipped with a 7.1 T magnet and operating at a ^{1}H Larmor Frequency of 299.17 MHz with a spinning frequency of 10 kHz. A 90° flip angle was used; 16k datapoints with a dwell of 3.33 μs were collected after a dead time of 6.67 μs. 256 acquisitions with a repetition time of 4 s were accumulated. The background signal obtained from a measurement under the same conditions on an empty rotor was subtracted from the signal. The proton NMR signal, including the spinning sidebands, was calibrated by the standard-addition method: first a proton spectrum of the glass with unknown water content is collected; then, known amounts of water are consecutively added to the sample and NMR spectra are collected intermittently to build the calibration curve (i.e. the NMR intensity versus the amount of water added); the initial water content is then determined by extrapolating the calibration curve to zero NMR intensity. In addition to the ^{1}H NMR, proton to silicon cross polarization (CP) experiments (Hartmann and Hahn, 1962) were performed for different contact times

to investigate if the water is preferentially associated with a specific silicon site. The CP spectra were acquired on a Varian Infinity spectrometer equipped with a 7.1 T magnet and operating at a ^{1}H Larmor Frequency of 299.17 MHz, a ^{29}Si Larmor Frequency of 59.42 MHz and a spinning frequency of 10 kHz. 4k datapoints with a dwell of 25 μs were collected after a dead time of 6.67 μs. 2560 acquisitions with a repetition time of 2 s were accumulated for different contact times in the range 0.1–7 ms. During the contact period, and amplitude modulation with a tangential shape (Hediger et al., 1995) was applied to the ^{29}Si channel. This optimizes the amount of polarization transferred from ^{1}H to ^{29}Si and makes the transfer robust towards fluctuations in the rf amplitude during cross polarization.

According to a study by Bourgue and Richet (2001), K_2O rich potassium silicate glasses have a strong tendency to retain CO_2 in their structure. In order to investigate the CO_2 content, selected, K_2O rich glasses have been analyzed by coulometry with a Coulomat 702-SO/CS/E at the Center of Mineral Analysis of the University of Lausanne. The sample was heated at 1300 °C under a flow of O_2. The released CO_2 is sent through a $Ba(ClO_4)_2$ solution, which decreases the pH by the formation of $BaCO_3$ from $Ba(OH)_2$. The pH is then restored by the addition of electrons to the solution. The quantity of current necessary to restore the pH is directly proportional to the amount of CO_2 in the sample. Typically, ~200 mg of sample were heated for 30 min at 1300 °C (the maximum furnace temperature). No additional CO_2 was exsolved for longer dwells at this temperature.

3.2. Calorimetry

The glass transition temperature, T_g, was determined by calorimetry on a Netzsch STA 449 C Jupiter in the Differential Scanning Calorimetry (DSC) mode. Approximately 30 mg of sample was put in a covered Pt90Rh10 crucible and the analysis was done with a heating rate of 10 K/min under a flow of argon. Because of the strong tendency for crystallization, the glasses could not be analyzed after a controlled cooling rate. However, all samples were prepared in equally sized batches and quenched in the same way, thus with the same cooling rate. A rapid increase of the heat capacity was observed at the glass transition. T_g was taken as the onset of the jump in the heat capacity at the glass transition. The uncertainty of the determination of the onset temperature from the DSC curves was estimated to be ±5 K.

3.3. ^{29}Si single quantum (SQ) MAS NMR

The ^{29}Si SQ MAS NMR spectra were acquired on a Varian Infinity spectrometer equipped with a 7.1 T magnet and operating at a ^{29}Si Larmor Frequency of 59.61 MHz with a spinning frequency of 15 kHz; no spinning sidebands were observed at this spinning frequency. A pulse width of 1.0 μs (20° flip angle) was used; 1024 datapoints were collected after a dead time of 20 μs with a dwell of 20 μs. A typical experiment consisted of 7200 acquisitions with a repetition time of 1 s. The repetition time of 1 s is shorter than 5 times the spin–lattice relaxation time ($T_1 \sim 3$ s), but a small flip angle (20°) was used and no differential relaxation of the various species was observed in spectra taken with different repetition times (0.1–32 s). TMS was measured as an external shift standard. No apodization was applied prior to the Fourier transform.

3.4. ^{29}Si double quantum (DQ) MAS NMR

3.4.1. Principles

The principles and applications of 2D DQ MAS NMR spectroscopy have been described extensively (e.g. Ernst et al., 1987) and do not need to be repeated here. In the present study, the J coupling between pairs of ^{29}Si is used to investigate the connectivity between the different sites. The J coupling is a through-bond interaction, thus, only ^{29}Si pairs that are chemically bonded to each other through a single oxygen will be observed in the spectra.

3.4.2. Experimental conditions

The two-dimensional ^{29}Si MAS NMR spectra were acquired using refocused INADEQUATE experiments (Bax et al., 1980, 1981; Lesage et al., 1999). The pulse sequence is shown in Fig. 1. The refocused INADEQUATE pulse sequence is particularly adequate for the investigation of disordered solids (Lesage et al., 1999) and, in addition, has been applied successfully for structure determinations of zeolites (Fyfe et al., 1990). The spectra were collected on ~100 mg of ^{29}Si enriched samples in 4 mm zirconia rotors on a Varian Infinity spectrometer equipped with a 7.1 T magnet and operating at a ^{29}Si Larmor Frequency of 59.61 MHz with a spinning frequency of 10 kHz. 256 t_2 datapoints with a dwell of 20 μs were collected for 64 t_1 increments with a dwell of 40 μs. For the experiments with $\Delta = 16$ ms, 256 acquisitions with a repetition time of 2 s were collected for each t_1 increment (total experiment time is 19 h). For the experiment with $\Delta = 46$ ms, 1024 acquisitions were collected for each t_1 increment (total experiment time is 80 h). All 2D spectra were processed in the same way: the t_2 dimension was zero-filled to 1024 points and a Gaussian apodization of 64 Hz was applied; the t_1

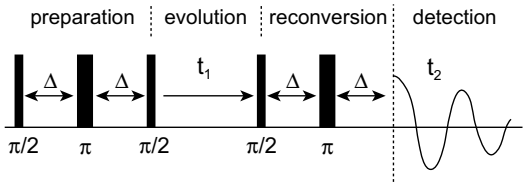

Fig. 1. Pulse sequence for solid state, refocused INADEQUATE. The double quantum coherence is created during a preparation interval 2Δ, evolves for a variable time interval t_1, is refocused into in-phase, single quantum magnetization during a reconversion interval 2Δ and is finally detected during a time t_2. Under ideal conditions, the degree of conversion into double quantum coherence is maximum for $\Delta = 1/4J_{SiSi}$, with J_{SiSi} equal to the strength of the J coupling. The reconversion pulses were phase cycled using a standard phase cycle (Ernst et al., 1987) to selectively filter double quantum coherences.

dimension was zero-filled to 256 points and a Gaussian apodization of 32 Hz was applied.

4. RESULTS

4.1. Sample composition

Where available, there is an excellent agreement between the EPMA or XRF analysis and the values expected from the sample preparation for the K_2O/SiO_2 ratio (Table 1); for the rest of the paper, the latter values will be used.

The ^{1}H NMR results indicate that the potassium metasilicate sample contains 0.76 wt% H_2O. At most, i.e. if all protons are present as Si–OH groups, this will increase NBO/T from 2.00 to 2.07. Because of their lower hygroscopicity, other samples are expected to have lower water contents.

The ^{29}Si signal intensity in the CP spectra is ~56 times lower than in the one pulse measurement on ^{29}Si. This low intensity can either be due to low ^{1}H concentrations, large ^{1}H/^{29}Si distances or inefficient polarization transfer (e.g. because of highly mobile H_2O). As polarization transfer from ^{1}H to ^{29}Si usually is not a problem in hydrous silicate minerals and glasses (e.g. Oglesby and Stebbins, 2000; Schmidt et al., 2000; Xue and Kanzaki, 2004) and typically leads to an increase in signal to noise, the low CP intensity for our sample must be due to low ^{1}H concentrations or large ^{1}H/^{29}Si distances. This is consistent with most of the water being detached from the bulk of the glass network, i.e. in a thin hydrated surface layer on the glass grains. In order to check if protons are preferentially bonded to a specific Si site, CP measurements with different contact times (from 0.1 to 7 ms) have been carried out. No changes in the relative peak intensities have been observed between the spectra from the CP with different contact times and the direct measurement. This demonstrates that the protons are not preferentially associated with a specific silicon site. Thus, the results of the ^{1}H NMR and the CP measurements indicate that contamination of the samples with water is small and will only have a minor effect on the glass structure, spectra and properties.

The CO_2 content was measured for a few selected samples and the results are shown in Table 1. The highest measured CO_2 content is 0.81 wt%. Bourgue and Richet (2001) have shown that CO_2 can be retained in potassium rich glasses for temperatures up to 1500 °C and the furnace temperature for the CO_2 analysis was limited to 1300 °C. Thus, the reported CO_2 contents are minimum values. Based on the data by Bourgue and Richet (2001), the maximum amount of CO_2 that is still retained in the melts at

Table 1
Sample compositions "as prepared" and measured by XRF (in brackets), glass transition temperatures, T_g and CO_2 content

No.	SiO_2 (wt%)	M_2O (wt%)	Fe_2O_3 (wt%)	T_g (K)	CO_2 (wt%)
Potassium silicate glasses (natural abundance ^{29}Si)					
1	79.20 (78.95)	20.70 (20.92)	0.10 (0.13)	785	N.A.
1[a]	(78.78)	(21.10)	(0.12)		
2	71.77 (71.27)	28.13 (28.57)	0.10 (0.16)	741	N.A.
3	71.77 (72.06)	28.13 (27.78)	0.10 (0.16)	N.A.	N.A.
4	65.61 (65.25)	34.29 (34.60)	0.10 (0.15)	745	0.05
5	60.90 (60.39)	39.00 (39.46)	0.10 (0.14)	N.A.	N.A.
6	60.43 (59.76)	39.47 (40.08)	0.10 (0.16)	773	N.A.
7	56.37 (54.85)	43.53 (44.98)	0.10 (0.17)	761	N.A.
8	56.01 (55.63)	43.89 (44.21)	0.10 (0.15)	N.A.	N.A.
9	50.95 (50.04)	48.95 (49.82)	0.10 (0.15)	N.A.	N.A.
10	50.46 (N.A.)	49.44 (N.A.)	0.10 (N.A.)	747	0.39
11	45.91 (44.95)	53.99 (54.87)	0.10 (0.18)	723	0.81
12	45.77 (45.15)	54.13 (54.68)	0.10 (0.17)	N.A.	N.A.
13	42.12 (41.58)	57.78 (58.27)	0.10 (0.15)	730	0.64
14	38.91 (37.63)	60.99 (62.15)	0.10 (0.22)	739	0.42
Potassium silicate glasses (96.74% ^{29}Si)					
15	47.21 (N.A.)	52.79 (N.A.)	0.10 (N.A.)	N.A.	N.A.
16	43.19 (N.A.)	56.81 (N.A.)	0.10 (N.A.)	N.A.	N.A.
17	39.30 (N.A.)	60.70 (N.A.)	0.10 (N.A.)	N.A.	N.A.
Rubidium silicate glasses					
18	39.13 (N.A.)	60.87 (N.A.)	0.10 (N.A.)	728	N.A.
19	24.32 (N.A.)	75.68 (N.A.)	0.10 (N.A.)	721	N.A.
Cesium silicate glasses					
20	29.90 (N.A.)	70.10 (N.A.)	0.10 (N.A.)	729	N.A.
21	17.57 (N.A.)	82.43 (N.A.)	0.10 (N.A.)	[b]	N.A.

N.A., not analyzed.
[a] EPMA analysis.
[b] T_g could not be determined due to crystallization.

1300 °C is estimated to be 0.88 wt%. However, as we measured lower CO_2 retention up to 1300 °C, we also expect smaller amounts of CO_2 to be retained above 1300 °C compared to the Bourgue and Richet (2001) samples. Thus, the highest CO_2 content in our samples is in the range 0.81–1.69 wt%. At most, i.e. if the CO_2 content is at the top of the expected range and if all carbon is present as carbonate groups, this will decrease NBO/T from 1.50 to 1.40. Thus, the CO_2 content will only have a limited effect on the glass structure, spectra and properties.

4.2. Calorimetry

The glass transition temperatures are listed in Table 1. They span a range between 723 and 785 K and are plotted as a function of the K_2O content in Fig. 2a. Because all samples have the same thermal history, any trend in T_g is due to differences in composition and not to differences in quench rates. Based on the viscosity data by Bourgue and Richet, the dissolved CO_2 can potentially decrease T_g by at most ~15 K for our range in CO_2 contents. Any potential changes in T_g due to dissolved CO_2 are expected to be a monotonic function of the K_2O content. For the K-silicate glasses, the T_g values show an overall decrease with increasing potassium content. However, T_g is not a monotonic function of the potassium content: there are local maxima of T_g around the di- and metasilicate composition. Due to differences in sample preparation (e.g. quench rates), measurement conditions (e.g. heating rates) and the characteristic points on the DSC curve chosen to define T_g, it is generally difficult to compare absolute values for T_g between different studies. Nevertheless, there is a reasonable agreement with previous studies for the K_2O range where data is available (Fig. 2a). Shelby (1976) measured the T_g of K-silicate glasses in the range 10–37 mol% K_2O; contrary to our results, no T_g maximum was observed at the disilicate composition. However, T_g was found to be nearly constant in the range 24–36 mol% K_2O, in contrast to a monotonous decrease they observed in the Na-silicate system. The data by Borisova et al. (1999) points to a similar conclusion, i.e. a relatively high T_g for K-silicate glasses at the disilicate composition compared to the Na-silicate system. Masnik et al. (1993) obtained values for T_g from the discontinuity in the curves of the Brillouin shift as function of temperature. They did not report the actual values but noted that "For binary systems, we find the highest glass transition temperature at the composition with 67.5% SiO_2" which is very close to the disilicate composition and consistent with our results.

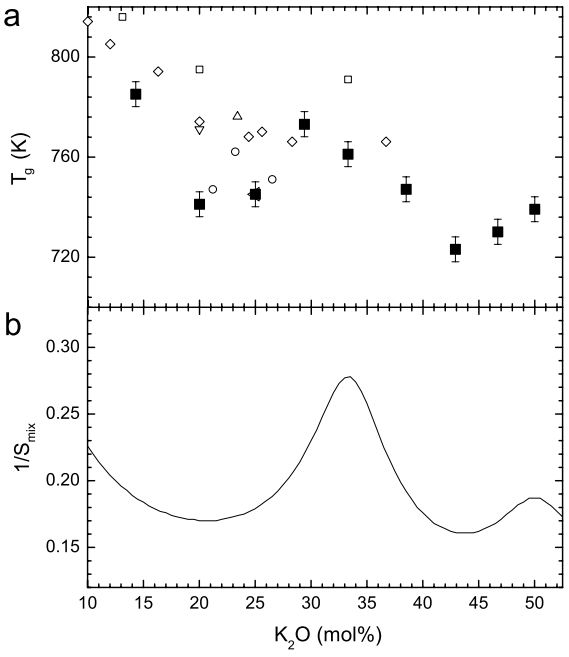

Fig. 2. (a) The glass transition temperature as a function of composition. The results from previous studies are shown for comparison (■, this study; ○, Dietzel and Sheybany (1948); Δ, Boesch and Moynihan (1975); ∇, Sasek et al. (1975); ◆, Shelby (1976); ◁, Bershtein et al. (1980); □, Borisova et al. (1999)). The large scatter between different studies is due to differences in sample preparation, measurement conditions and the different characteristic points on the DSC curves chosen to define T_g. (b) The inverse of the entropy of mixing as a function of composition. For both $1/S_{mix}$ and T_g, there are local maxima at the di- and metasilicate composition.

4.3. ^{29}Si single quantum MAS NMR

The spectra for nine samples in the K_2O–SiO_2 system are given in Fig. 3. Several effects with increasing potassium content can be observed: a shift of all the peaks to less negative ppm values, a change in the relative peak intensities and the appearance of new peaks. Olivier et al. (2001) interpreted the shift of the Q^n peaks with increasing potassium content as the result of a decreasing amount of Si in the second shell of cations (i.e. the fourth shell in total) around the central Q^n. They described this in terms of a change in the $Q^{n,jklm}$ distribution, where the additional superscripts denote the Q group character of the bonded tetrahedra. These different $Q^{n,jklm}$ species have different resonance frequencies, thus a change in their relative proportions results in an overall shift in the Q^n peak. For example, Q^3 consisting predominantly of $Q^{3,222}$ (typical for a potassium rich glass) is shifted to less negative ppm values compared to Q^3 consisting predominantly of $Q^{3,444}$ (typical for a silica rich glass). An alternative interpretation for this shift would lie in a change of the Si–O–Si bond angles with increasing potassium content, which would result in a subsequent change in the chemical shift (e.g. Smith and Blackwell, 1983). The spectra for the K-, Rb- and Cs-silicate glasses are shown in Fig. 4. For a given M^+/SiO_2 ratio (or NBO/T), the spectra of the alkali-silicate glasses are shifted towards more negative ppm values in the series K–Rb–Cs. The magnitude of the shift is correlated with the inverse of the radius r of the cation (see Fig. 5 for the metasilicate samples).

4.3.1. Peak assignment

The bands with average positions at −104, −92, −83 and −73 ppm can be confidently assigned to Q^4, Q^3, Q^2 and Q^1, respectively (Maekawa et al., 1991). The assignment is

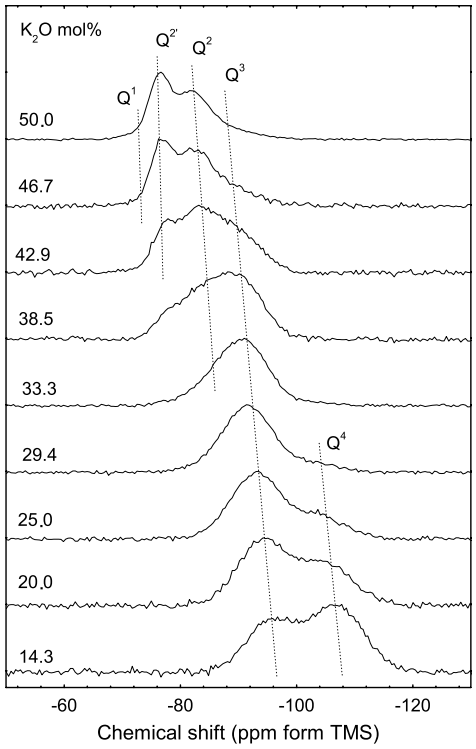

Fig. 3. [29]Si MAS NMR spectra of potassium silicate glasses. The assignment of the various bands is indicated by the lines (guides to the eye only). Note the continuous shift in peak position as a function of composition (see text).

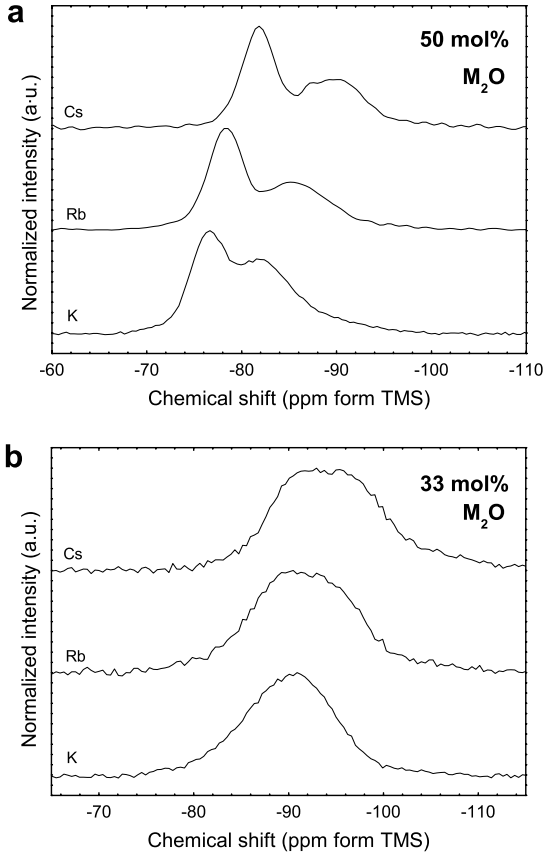

Fig. 4. [29]Si MAS NMR spectra of potassium, rubidium and cesium metasilicate (a) and disilicate (b) glass.

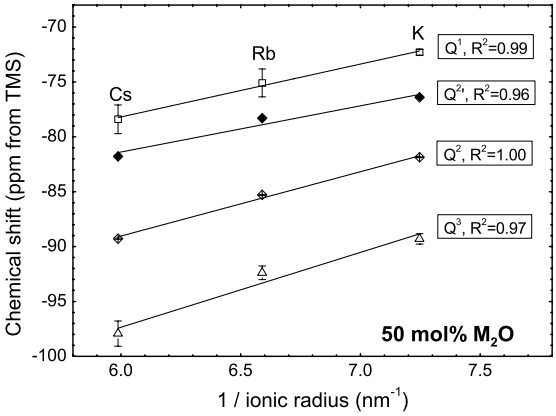

Fig. 5. The [29]Si chemical shifts of potassium, rubidium and cesium metasilicate glasses as a function of 1/ionic radius. The effective ionic radii were taken from Shannon (1976) for a coordination number of 6.

indicated in Fig. 3. The assignment of the narrower peak at an average position of −77 ppm, which is also present in the spectra of the Rb- and Cs-metasilicate glasses (Fig. 4a), is more problematic. Dupree et al. (1984) assigned the peak to Q^1, however, this assignment is not consistent with the stoichiometry of the glasses, i.e. there would be insufficient potassium cations available to charge balance all the NBO. The assignment to a Q^2 species is consistent with the stoichiometry of the glasses, i.e. the amount of NBO calculated from the Q^n speciation is equal to the amount of potassium cations, and Maekawa et al. (1991) tentatively assigned the peak to a Q^2 species in a specific ring configuration ($Q^{2'}$), but they did not investigate this any further.

4.3.2. Curve fitting and species abundance

The spectra were fitted with Gaussian peaks, using a Levenberg–Marquardt algorithm to minimize χ^2. The use of constraints on peak position, width or amplitude was avoided as much as possible. In a few cases however, it was necessary to constrain the peak position or width to obtain a meaningful fit. The use of constraints is indicated in Table 2. For example, the chemical shift of Q^1 in the Cs-metasilicate glass has to be fixed to obtain a meaningful fit -this was done by extrapolating the values obtained from the K- and Rb-glasses but the resulting fit remains inherently dependent on the value of this constraint. The high degree of overlap of the peaks in the spectra of the Rb- and Cs-disilicate glasses (Fig. 4b), and the lack of information on peak widths and positions from spectra for other compositions, prevent a meaningful fit of these spectra altogether. The abundance of each species is obtained by dividing its peak area by the sum of the area's of all peaks. The abundances of the species obtained from the curve fitting (Table 2) are in good agreement with those obtained by Maekawa et al. (1991). The NBO/T calculated from

Table 2
Fits without constraints on peak area's: chemical shift (σ, ppm), half width at half maximum (hwhm, ppm) and Q^n abundance (A, %)

No.	M_2O (mol%)	Q^4			Q^3			Q^2			$Q^{2'}$			Q^1			NBO/T (comp.)	NBO/T (NMR)
		σ	hwhm	A	σ	hwhm	A	σ	hwhm	A	σ	hwhm	A	σ	hwhm	A		
Potassium silicate glasses																		
1	14.3	−106.9	5.5	59.8	−95.5	4.9	40.2										0.33	0.40
2	20.0	−104.8	5.7	43.2	−93.9	4.9	56.8										0.50	0.57
3	20.0	−104.8	5.5	41.7	−93.6	5.1	58.2										0.50	0.58
4	25.0	−104.2	5.0	24.6	−93.0	5.1	75.4										0.67	0.75
5	29.0	−103.5	4.4	11.1	−91.3	5.2	88.9										0.82	0.89
6	29.4	−103.4	4.0	8.3	−91.7	5.1	89.5	−83.1[a]	3.5	2.2							0.83	0.94
7	33.0	−104.0	4.2	3.1	−90.2	5.1	83.8	−83.0[a]	5.1	13.1							0.99	1.10
8	33.3	−104.1	3.4	2.6	−90.7	5.1	85.4	−83.0[a]	5.0	12.0							1.00	1.09
9	38.0				−90.2	4.7	58.0	−83.6	4.6	36.3	−77.2	2.4	5.7				1.23	1.42
10	38.5				−90.3	4.7	55.9	−82.9	4.5	37.7	−77.2	2.4	6.5				1.25	1.44
11	42.9				−89.9[a]	4.8	37.3	−82.6	4.1	47.1	−76.9	2.1	13.4	−72.6	3.6	2.2	1.50	1.65
12	43.0				−89.9	4.5	35.2	−82.6	4.0	48.4	−76.9	2.3	16.2				1.51	1.64
13	46.7				−89.0[a]	5.6	22.3	−82.0	3.9	49.3	−76.5	2.0	24.9	−72.9	3.9	3.5	1.75	1.81
14	50.0				−89.0[a]	5.3	14.2	−81.7	3.7	49.5	−76.3	2.0	31.6	−72.4	2.9	4.8	2.00	1.91
Rubidium metasilicate glass																		
19	50.0				−93.2	5.3[a]	6.2	−85.3	4.1	43.7	−78.3	2.0	40.9	−75.6	3.5	9.2	2.00	2.03
Cesium metasilicate glass																		
21	50.0				−98.6	5.3[a]	4.2	−89.3	3.9	46.8	−81.8	1.9	44.1	−78.4[a]	2.4[b]	4.9[b]	2.00	2.01

[a] Constrained value.
[b] Results are very dependent on the constraint for $\sigma(Q^1)$.

composition (NBO/T $= 2 \cdot [K_2O]/[SiO_2]$) and the speciation (NBO/T $= 3 \cdot [Q^1]+2 \cdot [Q^2]+3 \cdot [Q^3]$) show a reasonable agreement (Table 2). However, this unconstrained fitting of the NMR spectra consistently overestimates the amount of NBO. This cannot be due to the presence of water as this overestimation of NBO/T is also the case for SiO_2 rich glasses that are not hygroscopic.

In a second round of fitting, we have constrained the peak area's such that the NBO/T calculated from the fit is equal to the NBO/T calculated from the compositions (Table 3). An example of such an area-constrained fit is shown in Fig. 6. The goodness of fit parameter χ^2 for the area-constrained fits is only marginally higher than for the unconstrained fits and the residuals are mostly indistinguishable. Furthermore, less constraints on peak positions and widths were necessary to obtain reasonable fitting results. In addition, the scatter on the peak area's and widths as a function of the composition is significantly lower for the area-constrained fits. This indicates that the area-constrained fits (Table 3) are a better representation of the speciation in the glasses. For the remainder of the paper, the results of the area-constrained fits will be used; but very similar results were obtained by using the results from fits where the areas were not constrained (Table 2).

4.3.3. Speciation reaction

The measured speciation (with $[Q^2_{\text{total}}] = [Q^2] + [Q^{2\prime}]$) is plotted as a function of NBO/T in Fig. 7. An exact calculation of the error on the speciation is difficult, but considering the uncertainty in the phasing of the spectra, the choice of Gaussian lineshapes and the curve fitting, the absolute uncertainty on the determination of the abundances of the species is estimated to be a few %. Note that because T_g depends on the composition for a given quench rate, this plot is not "isothermal", i.e. the measured speciation of the glasses represents the speciation of the melts at T_g, which is at different temperatures for different compositions. However, the range in T_g is small (Fig. 2) and hence also the expected effect of different T_g's on the speciation (e.g. Brandriss and Stebbins, 1988; Mysen and Frantz, 1992; McMillan et al., 1992; Malfait et al., 2007).

The natural logarithm of equilibrium constant K_2 of reaction (1) with $n = 2$ are plotted as a function of $1/r$ in Fig. 8. The results from Maekawa et al. (1991) for Li-, Na- and K-metasilicate glasses are also plotted for comparison. There is a correlation between $\ln(K_2)$ and $1/r$. This correlation has been observed before for Li-, Na- and K-silicate glasses (e.g. Brawer and White, 1975; Emerson et al., 1989; Maekawa et al., 1991; Mysen and Frantz, 1992); our data indicates that this trend is also valid for Rb- and Cs-silicate glasses.

4.4. ^{29}Si INADEQUATE experiments

^{29}Si INADEQUATE experiments were used to investigate the medium range structure of the glasses: the connectivity between the different species and the nature of the additional peak for Q^2.

4.4.1. Interpretation of 2D spectra

The interpretation of the 2D DQ spectra will be explained with a schematic spectrum (Fig. 9). In the two-dimensional DQ/SQ spectrum (Fig. 9a), the horizontal axis ($\omega 2$) is the SQ dimension that contains the chemical shift information, i.e. the value on the X axis of a peak is the chemical shift of a single spin. The vertical axis ($\omega 1$) is the DQ dimension that contains the information about the spin pair, i.e. the value on the Y axis of a peak in the spectrum is the sum of the chemical shifts of two coupled spins. A pair of spins with identical chemical shifts (ω_A) will have one peak in the 2D spectrum at the coordinate $(\omega_A, 2\omega_A)$, i.e. it is on the DQ–SQ diagonal. A pair of spins with a different chemical shift (ω_A and ω_B) will have two peaks in the 2D spectrum at the coordinates $(\omega_A, \omega_A + \omega_B)$ and $(\omega_B, \omega_A + \omega_B)$; they are off-diagonal with respect to the DQ–SQ diagonal. The DQ–SQ correlation spectrum can be transformed to a symmetric correlation spectrum (Fig. 9b) through a shear transformation, which is nothing more than a linear transformation of the data (Ernst et al., 1987). Clearly, the sheared spectrum should be symmetrical around the diagonal. The sheared and unsheared spectra contain the same information, but the sheared spectra give a better visual representation of the information. Thus, only the sheared spectra will be shown, the unsheared spectra can be found in Electronic annex EA-1.

4.4.2. ^{29}Si INADEQUATE spectra

The one-dimensional, J-filtered spectra of the potassium metasilicate glass are plotted for various delay times Δ in Fig. 10. The overall decrease in intensity with increasing Δ is due to T_2 relaxation during the pulse sequence. The relative intensity of the peak at -77 ppm, compared to the -82 peak, increases as a function of Δ. This indicates weaker J couplings for the -77 ppm peak compared to the -82 ppm peak, assuming similar transverse relaxation rates for both peaks. Because of the different J couplings for different Si sites, the relative intensities in the two-dimensional INADEQUATE spectra are no longer quantitative in nature. In particular, the intensity of the -77 ppm peak will be low in the 2D spectra due to the weaker J coupling.

The sheared, 2D spectra for different compositions and different values of Δ are shown as contour plots in Fig. 11b; the projections along the single and double quantum dimension are also shown. As expected, the sheared spectra are symmetrical around the diagonal. The one-pulse spectra are plotted in Fig. 11a for comparison. Vertical cross-sections through the SQ–SQ correlation spectra at the peak positions of Q^2 and $Q^{2\prime}$ are shown in Fig. 11c and d, respectively. These slices represent the chemical shifts from sites coupling to Q^2 and $Q^{2\prime}$, respectively. Just as for the SQ spectra, the 2D spectra consist of broad, highly overlapping peaks. For this reason, we will look in more detail at the cross-sections (Fig. 11c and d) first and consider the 2D spectra later.

It is clear from Fig. 11c that Q^2 is connected to Si with a chemical shift of -82 ppm, i.e. Q^2 is connected to itself, and to Si with a chemical shift of -91 ppm, i.e. Q^2 is connected to Q^3, with more Q^2–Q^3 connections at higher SiO_2 contents. No connection from Q^2 to $Q^{2\prime}$ (-77 ppm) is observed.

Table 3
Area-constrained fits: $(3Q^1 + 2Q^2 + Q^3)/100 = \text{NBO/T}$: chemical shift ($\sigma$, ppm), half width at half maximum (hwhm, ppm) and Q^n abundance (A, %)

No.	M_2O (mol%)	Q^4			Q^3			Q^2			$Q^{2'}$			Q^1			NBO/T = (comp.)	NBO/T (NMR)
		σ	hwhm	A	σ	hwhm	A	σ	hwhm	A	σ	hwhm	A	σ	hwhm	A		
Potassium silicate glasses																		
1	14.3	−106.3	6.1	66.7	−94.8	4.4	33.3										0.33	0.33
2	20.0	−104.0	6.4	50.0	−93.5	4.7	50.0										0.50	0.50
3	20.0	−104.3	6.3	50.0	−93.5	4.7	50.0										0.50	0.50
4	25.0	−102.7	6.3	33.3	−92.5	4.8	66.7										0.67	0.67
5	29.0	−101.6	6.3[a]	18.3	−91.5	5.0	81.7										0.82	0.82
6	29.4	−99.7	6.2[a]	19.5	−91.2	4.7	77.7	−82.8	3.0	2.8							0.83	0.83
7	33.0	−99.7	6.2[a]	7.7	−92.7	5.1	86.2	−83.7	3.6	6.2							0.99	0.99
8	33.3	−99.7	6.2[a]	5.7	−90.3	5.1	88.7	−81.1	3.7	5.7							1.00	1.00
9	38.0				−90.3	5.4	77.4	−82.7	4.0	18.0	−78.0	2.1	4.6				1.23	1.23
10	38.5				−89.0	5.5	75.0	−81.3	3.5	18.9	−76.9	2.2	6.1				1.25	1.25
11	42.9				−88.5	5.6	50.0	−81.6	4.3	39.4	−76.7	2.0	10.6				1.50	1.50
12	43.0				−88.9	5.5	49.1	−82.0	3.9	38.7	−77.1	2.0[a]	12.1				1.51	1.51
13	46.7				−87.8	6.1	28.0	−81.9	3.7	42.6	−76.6	2.0	26.3	−72.3[a]	3.6	3.0	1.75	1.75
17[b]	50.0				−89.3	4.9	10.0	−81.9	3.7	46.9	−76.4	2.0	33.0	−72.3[a]	3.7	10.0	2.00	2.00
Rubidium metasilicate glass																		
19	50.0				−92.4	5.7[a]	7.5	−85.3	4.0	42.5	−78.3	2.0	42.4	−75.1	3.3	7.5	2.00	2.00
Cesium metasilicate glass																		
21	50.0				−97.9	5.7[a]	4.7	−89.3	3.9	46.3	−81.8	1.9	44.3	−78.4	2.3	4.7	2.00	2.00

[a] Constrained value.
[b] No reasonable area-constrained fit could be obtained for spectrum 14, spectrum 17 was used in stead (same composition).

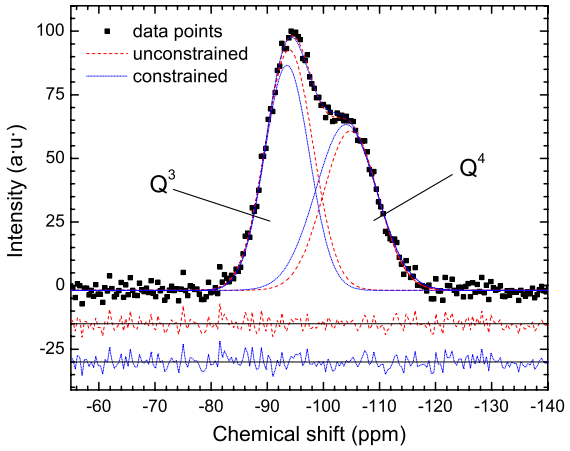

Fig. 6. ^{29}Si MAS NMR spectrum and 2 possible fits for the potassium tetrasilicate glass (20 mol% K_2O). For the constrained fit, the peak area's were fixed to satisfy the condition $3Q^1 + 2Q^2 + Q^3 = \text{NBO/T}$ with $\text{NBO/T} = 2\cdot[K_2O]/[SiO_2]$. The residual and χ^2 values are nearly identical for the constrained and unconstrained fit (χ^2 equals 5.35 and 5.68, respectively).

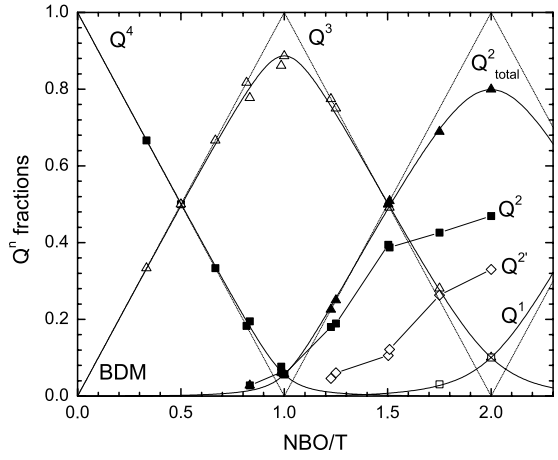

Fig. 7. Speciation as a function of NBO/T. The solid lines represent the Q^4, Q^3, Q^2_{total} and Q^1 speciation for $\log K_3$ and $\log K_2$ equal to -2.4 and -1.8, respectively. Dashed lines show the speciation for a binary distribution model (BDM), i.e. the speciation if the equilibrium constants K_n were equal to zero.

In addition, it is clear from Fig. 11d, that $Q^{2'}$ is connected to Si with a chemical shift of -77 ppm, i.e. $Q^{2'}$ is connected to itself, and to Si with a chemical shift of -85 ppm, which we will assign to $Q^{3'}$ (see below). There is a higher proportion of $Q^{2'}$–$Q^{3'}$ connections at higher SiO_2 contents, to the extent that at 42 mol% K_2O, only $Q^{2'}$–$Q^{3'}$ connections can be observed in the spectra. No connection from $Q^{2'}$ to Q^2 (-82 ppm) or Q^3 (-91 ppm) is observed. The weak shoulder at the Q^3 position that is present for the most silica rich sample (Fig. 11d4), most likely results from Q^2 species that have a chemical shift of -77 ppm, i.e. the species from the tail of the Q^2 Gaussian peak towards less negative ppm values (see Fig. 11a1). Because of the low $Q^{2'}$ contents in this sample and the weak J coupling for $Q^{2'}$, these Q^2 species will contribute significantly to the total intensity in the J coupled spectra at -77 ppm.

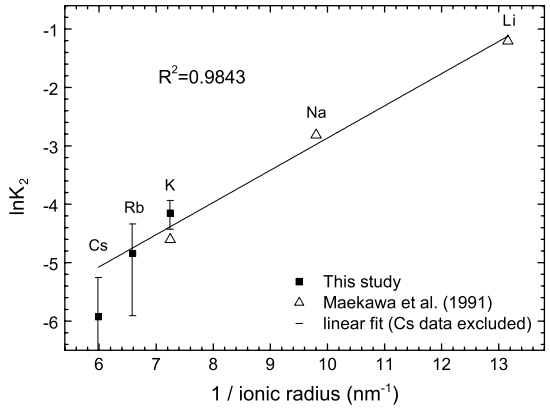

Fig. 8. Correlation between the equilibrium constant of the speciation reaction, $\ln(K_2)$, and the reciprocal of the ionic radius, r. The large uncertainty for the Cs data is due to the very small amounts of Q^1 and Q^3 present in the glass. Because of this large uncertainty, the Cs data were not included for the linear fit. No errors were presented in Maekawa et al. (1991). The effective ionic radii were taken from Shannon (1976) for a coordination number of 6.

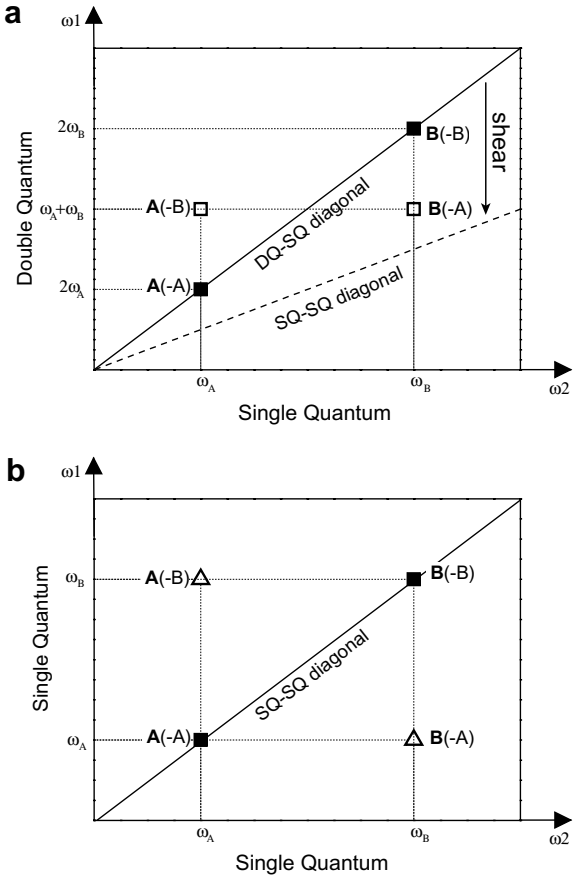

Fig. 9. Schematic DQ–SQ correlation spectrum (a) and its corresponding SQ–SQ correlation spectrum (b). The symmetric correlation spectrum is obtained from the DQ–SQ spectrum through a linear shear transformation.

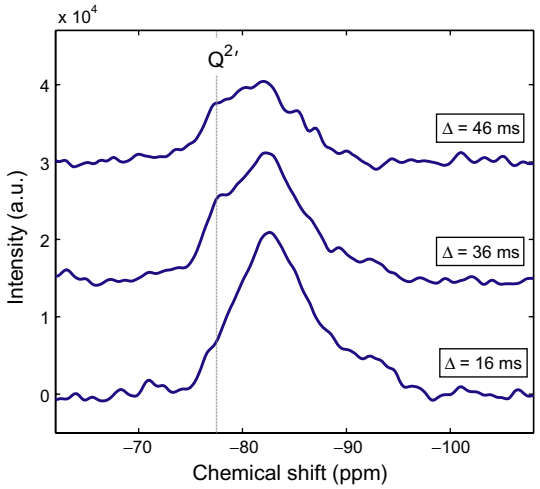

Fig. 10. *J*-filtered spectra of a potassium metasilicate glass for different values of Δ. The relative intensity at −77 ppm is larger for larger delays Δ, indicating weaker *J* couplings for $Q^{2'}$.

In the 2D spectra (Fig. 11b), several peaks and shoulders can be identified at positions that are consistent with the interpretation of the cross-sections, i.e. there are two, disconnected sets of species. The connectivity patterns are marked on the 2D spectra by the solid lines.

In conclusion, the DQ spectra and their cross-sections indicate that there are two sets of species, Q^n and $Q^{n'}$ ($n = 2,3$), which show no interconnection through the Q^2 and $Q^{2'}$ sites.

It should be noted that the presence of a second type of Q^3 species indicates that fitting the SQ spectra with a single Gaussian for Q^3 as was done in Section 4.3.2, inevitably introduces an error (estimated smaller than a few %) in the determination of the total amount of Q^3. Unfortunately, the strong peak overlap of $Q^{3'}$ with Q^2 and Q^3 in the SQ dimension and the uncertainty about the peak positions and widths, make a sensible fit of the SQ spectra with separate peaks for both Q^3 and $Q^{3'}$ impossible.

5. THREE-MEMBERED RINGS

As explained in the previous section, the DQ spectra demonstrate that there are two sets of Q^n and $Q^{n'}$ species ($n = 2,3$) which show no interconnection through $Q^{2'}$. This is a strong indication that $Q^{2'}$ is part of a distinct type of ring, since a $Q^{2'}$ species in a ring can only be connected to Q^n species that are part of the same ring. The $Q^{3'}$ peak is then assigned to a Q^3 that is part of the same type of ring. The $Q^{3'}$ assignment is based on the connection between $Q^{2'}$ and $Q^{3'}$ (evidenced by the cross-peaks in the 2D spectra). In addition, the difference in chemical shift between $Q^3/Q^{3'}$ and $Q^2/Q^{2'}$ is similar. The presence of $Q^{3'}$ in the Rb- and Cs-disilicate glass could be responsible for the small shoulder at ca. −90 ppm in their NMR spectra (Fig. 4b); no attempt, however, was made to fit this.

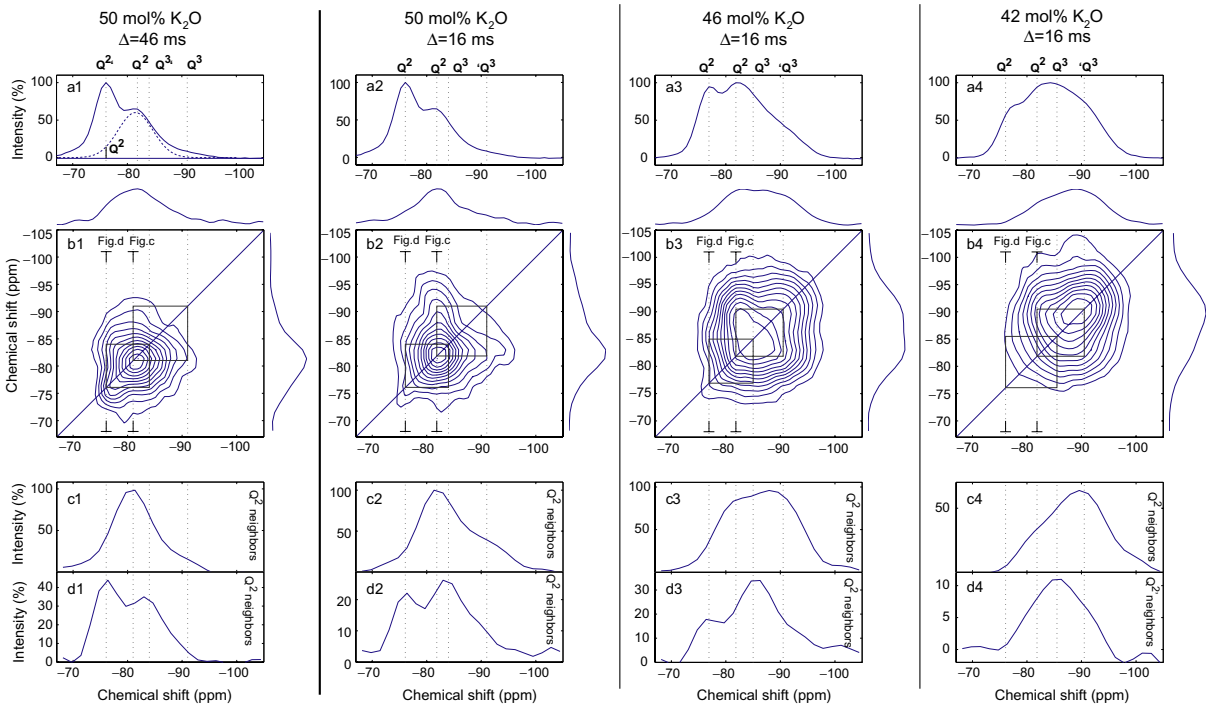

Fig. 11. Results from ^{29}Si INADEQUATE experiments. Single-pulse spectra (a), sheared *J* coupled correlation spectra (b), vertical cross-sections from the SQ–SQ correlation spectra at −81 ppm (c) and at −77 ppm (d). The slices in (c) and (d) represent the chemical shift from the sites coupled to Q^2 and $Q^{2'}$, respectively. Columns 1 and 2 are spectra from the same sample, but collected with different mixing times Δ in the pulse sequence; columns 2, 3 and 4 show spectra collected with the same parameters, but from glasses with different compositions. Contours were drawn along 12, equally spaced levels from 10% to 100% of the maximum intensity.

There is evidence from NMR spectroscopy that the ring structure containing $Q^{2'}$ and $Q^{3'}$ consists of three silica tetrahedra.

- The observed linewidth of the −76 ppm peak ($Q^{2'}$) is only half that of the Q^2 peak, indicating that there is less variation in the chemical environments around this species; this is consistent with a species with a constrained geometry, as is the case for a three-membered ring, which is expected to have a planar geometry (Galeener, 1982a,b).
- The small J couplings for the $Q^{2'}$ site (Fig. 10): for aqueous silicate solutions, Haouas and Taulelle (2006) have shown that the J couplings within three-membered rings are consistently small compared to J couplings in larger rings or chains.
- The similar difference in chemical shift for Q^2 species in chain and ring configurations in K-silicate aqueous solutions (Harris and Newman, 1977).
- The similar difference in chemical shift for Q^2 species in the α- and the β-form of $CaSiO_3$, known to consist of three-membered rings and chain configuration, respectively.
- The similar difference in chemical shift between Q^2 in three-membered and four-membered organosiloxanes (Casserly and Gleason, 2005).
- The Si–O–Si angles in three-membered rings are small (e.g. 136° in crystalline K_2SiO_3) compared to those in larger ring or chain structures. First-principles calculations of NMR parameters of sodium silicate glasses show that the isotropic chemical shift for Q^2 species are a function of the Si–O–Si angle, with a chemical shift of −76 ppm for small Si–O–Si angles (134°) and a chemical shift of −82 ppm for larger Si–O–T angles (147°) (Charpentier et al., 2004).

There are other indications that three-membered rings are present in K-, Rb- and Cs-silicate glasses:

- Werthmann and Hoppe (1981) showed that crystalline K_2SiO_3, Rb_2SiO_3 and Cs_2SiO_3 consists of $(Si_3O_9)^{6-}$ rings.
- Yasui et al. (1994) concluded from molecular dynamics calculations for alkali metasilicate glasses that if the cation is large, Si–O chain structures are modified to form small rings. They only observed this for Cs- and Rb-silicate glasses and not for K-silicate glasses however.
- Wicks et al. (1997) observed three-membered rings in molecular dynamics simulations of K-silicate glasses. Unfortunately, no ring statistics were presented and the amount of three-membered rings was constrained to be zero in their later models.
- Using molecular dynamics calculations, Machácek and Gedeon (2003) observed that the amount of three-membered rings in binary Rb- and Cs-silicate glasses with a bulk NBO per tetrahedral cation (NBO/T) of 0.86 increased with increasing cation size.
- Majerus et al. (2004) observed significant amounts of three-membered rings in the Reverse Monte Carlo (RMC) simulations of in-situ, high-temperature neutron diffraction data of disilicate glasses and melts. The amount of three-membered rings was highly dependent on the initial configurations, but increased with increasing temperature for both types of models used.
- In the Raman spectra of Li-, Na-, K-, Rb- and Cs-silicate glasses, Matson et al. (1983) found that with increasing alkali content, the relative intensity of the band at ~600 cm^{-1} (generally attributed to three-membered rings, e.g. Galeener, 1982a,b or Kubicki and Sykes, 1993), decreases in the spectra of Li-silicate and possibly Na-silicate glasses, whereas the intensity of this band increases for the K-, Rb- and Cs-glasses in the order Cs > Rb > K.

Furthermore, large alkali ions also seem to induce the formation of three-membered rings in more polymerized glasses and melts:

- Using IR spectroscopy, Simakin et al. (2004) observed a linear correlation between the area of the peak attributed to three-membered rings, and the alkali cation radius for feldspathoid glasses containing Na, K and Rb, respectively.
- McMillan et al. (1998) observed an increased area of the peak near 560 cm^{-1}, attributed to three-membered rings in the Raman spectra of fully polymerized Rb- and Cs-aluminosilicates, compared to the Li, Na and K analogues.

The DQ results, corroborated by information from the literature, thus provide strong evidence for the presence of large amounts of three-membered rings in the alkali rich K-, Rb- and Cs-silicate glasses. Fig. 12 shows a schematic illustration of such a three-membered ring and the various Q^n and $Q^{n'}$ species.

The abundance of Q^2 in three-membered ring structures, $Q^{2'}$, can be measured directly from the SQ spectra and

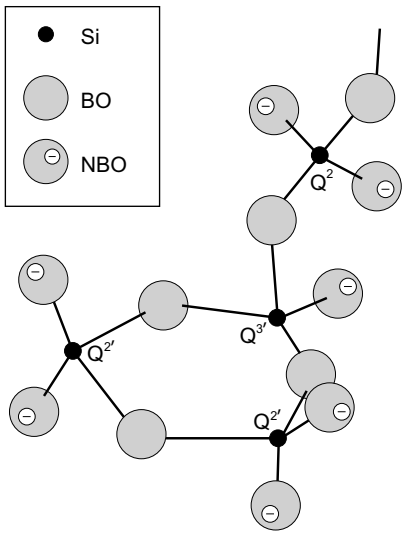

Fig. 12. Schematic illustration of a three-membered ring and the different Q^n and $Q^{n'}$ species.

increases with increasing radius of the alkali cation (Fig. 13). The maximum amount of $Q^{2'}$ that was measured is 44% in the Cs-metasilicate glass. Due to highly overlapping peaks, the amount of Q^3 and Q^4 in three-membered rings, and thus the total amount of rings, cannot be quantified directly from the NMR results.

However, it can be estimated under the assumption that all silica has the same tendency to go into three-membered rings as Q^2 (apart from Q^1 and Q^0 of course, which cannot be part of any type of ring). The tendency for Q^2 to go into rings ($[Q^{2'}]/[Q^2_{\text{total}}]$) was calculated from the NMR results for glasses with high K_2O content. The amount of rings in pure SiO_2 glass was set to be zero, consistent with Galeener, 1982a,b who estimated the amount of rings in vitreous silica to be in the order of ~1%. The fraction of silica in three-membered rings is estimated over the entire compositional range by fitting the data with a simple exponential function (Fig. 14). It should be noted that the choice of an exponential function to fit the data is rather arbitrary and the obtained values for the fraction of rings are mere estimates (especially so in the compositional range where no quantitative information is available). The presence of silica in three-membered rings at lower alkali content is qualitatively supported by the double quantum results ($Q^{3'}$ species detected), molecular dynamics simulations at the disilicate composition (Majerus et al., 2004) and the 590 cm^{-1} peak intensities in the Raman spectra of K-, Rb- and Cs-silicate glasses (Matson et al., 1983).

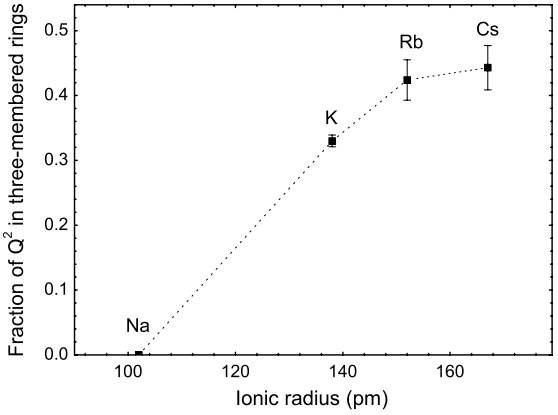

Fig. 13. The absolute amount of $Q^{2'}$ in three-membered rings as a function of ionic radius of the modifier cation (line is drawn as guide for the eye).

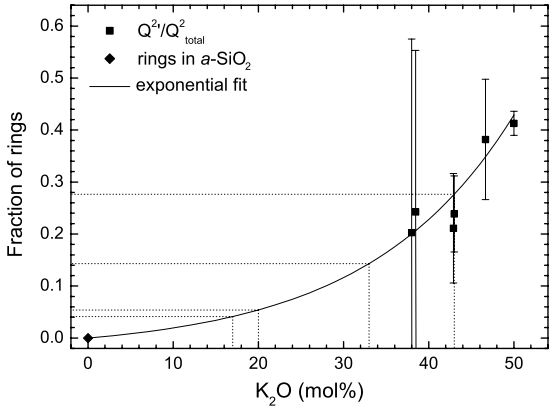

Fig. 14. Fraction of three-membered rings as a function of K_2O content. The squares are the amount of $Q^{2'}$ in three-membered rings, the diamond is the amount of three-membered rings in SiO_2 glass, set equal to 0 (see text). The dotted lines mark the compositions for which heat capacity data is available (Richet and Bottinga, 1985), the amount of rings for these compositions was estimated from the fit to the NMR data.

6. VARIATIONS IN MELT STRUCTURE

The strong correlation between the chemical shifts and $1/r$ (Fig. 5) indicates that the electron density around Si, and thus also the strength of the $Si–O_{NBO}$ bond, depends on the electrostatic potential ($\sim 1/r$) around the different modifiers. Turner et al. (1986) observed a similar correlation between the ^{31}P chemical shift and cationic field strength in orthophosphates with different cations.

The observed correlation between $\ln(K_2)$ and $1/r$ (Fig. 8) for the metasilicate glasses indicates that it is the electrostatic interaction between the negatively charged NBO within a SiO_4 tetrahedron that determines the equilibrium constant; this observation is consistent with a model proposed by Gurman (1990). The amount of negative charge on the NBO depends on the electrostatic interaction of the NBO with the network modifier, thus also on $1/r$ of the modifier. A similar correlation between $\ln(K_3)$ and $1/r$ is to be expected, i.e. K_3 is expected to decrease in the series $K < Rb < Cs$.

The increase of $Q^{2'}$ from three-membered ring structures with increasing radius of the alkali cation (Fig. 13) indicates that the accommodation of large alkali ions in the structure becomes increasingly more difficult with increasing cation size; this apparently causes an increased tendency to form three-membered rings. This trend is qualitatively consistent with results from molecular dynamics simulations (Yasui et al., 1994; Machácek and Gedeon, 2003) and spectroscopic observations (McMillan et al., 1998; Simakin et al., 2004) on other systems. However, in the molecular dynamics simulations, the three-membered rings were only present in Rb- and Cs-silicate glasses, and not for K-glasses and they were always present in much smaller quantities. The quantification of the vibrational spectroscopic observations of these rings on the other hand was difficult due peak overlap and unknown scattering cross-sections and absorption coefficients.

7. STRUCTURE AND PHYSICOCHEMICAL PROPERTIES

7.1. Glass transition temperature

The Adam–Gibbs relaxation theory (Adam and Gibbs, 1965; Richet, 1984) describes the relation between the viscosity and the configurational entropy. Assuming that T_g occurs at 10^{12} Pa.s, Toplis (1998) rearranged the Adam–Gibbs relation to the equation

$$T_g = B_e/S_c(T_g) * 1/(12 - A_e) \quad (3)$$

where $S_c(T)$ is the configurational entropy, consisting of a chemical part due to mixing of species or components and a topological part due to variations in e.g. bond angles and lengths; B_e is related to the potential energy barrier to viscous flow; the physical meaning of A_e is less clear, but variations in A_e are generally limited.

Assuming ideal mixing behavior, the contribution of the entropy of mixing of the Q^n species to the configurational entropy can be calculated with

$$S_{mix} = -R \cdot \sum [Q^n] \ln [Q^n] \quad (4)$$

where R is the gas constant and $[Q^n]$ is the abundance of the different Q^n species. For Q^2, the total amount, i.e. the sum of $[Q^{2'}]$ and $[Q^2]$, was considered for S_{mix} since the difference between Q^2 and $Q^{2'}$ is only topological in nature (e.g. different Si–O–Si bond angle). If the mixing of the Q^n species, S_{mix}, is an important part of S_c, a relation between $1/S_{mix}$ and T_g is to be expected for the compositional range where the same viscosity mechanism (similar values for B_e) is important. This is exactly what is observed in Fig. 1b, where the entropy of mixing is plotted as a function of composition. Local minima and maxima occur at the same positions for both T_g and $1/S_{mix}$ as a function of composition. Toplis (1998) did not observe such a relation for Na-silicate glasses, possibly because the variations in S_{mix} for Na-silicate glasses are about 4 times smaller than for K-silicate glasses due to the larger equilibrium constants K_n. The correlation that was observed for the K-silicate glasses, indicates that the mixing of Q^n species contributes significantly to the configurational entropy and has a profound effect on T_g. The more silica rich glasses have a high T_g compared to $1/S_{mix}$. This is consistent with the idea that the mechanism of viscous flow in highly polymerized melts involves the breaking of strong Si–O–Si bonds as an initial step (McMillan et al., 1994), resulting in a high activation energy (thus a high B_e parameter and a higher T_g), whereas this is not the case in melts with sufficient NBO (Stebbins, 1995).

7.2. Heat capacity

Richet et al. (1984) and Richet and Bottinga (1985) observed an anomalous, non-linear composition and temperature dependence of the heat capacity of binary K-silicate melts, in contrast to the temperature independent, compositionally linear dependent heat capacity of Li- and Na-silicate melts (Fig. 15).

In order to investigate if the anomalous heat capacity behavior is related to the presence of three-membered rings, we modeled the heat capacity as a function of composition for three different temperatures. We considered the heat capacity of the melt to consist of two contributions: a temperature independent, compositionally linear dependent contribution

$$C_{p,linear} = [SiO_2] \cdot C^0_{p(SiO_2)} + [K_2O] \cdot C^0_{p(K_2O)} \quad (5)$$

as observed in Li- and Na-silicate melts, and a temperature dependent, compositionally non-linear dependent contribution that is caused by the presence of the strained, three-membered rings.

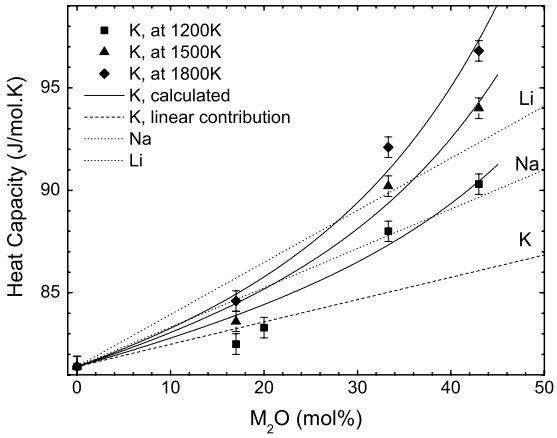

Fig. 15. The heat capacity (C_p) of Li-, Na- and K-silicate melts (data from Richet and Bottinga (1985), data on SiO_2 melt from Richet et al. (1982)). The C_p of K-silicate melts consists of a temperature independent, compositionally linearly dependent part (analogue to the C_p behavior of Li- and Na-silicate melts) and a temperature dependent contribution due to the three-membered rings.

$$C_{p,rings} = A(T) \cdot [Q^{total}_{rings}] \quad (6)$$

where $[SiO_2]$ and $[K_2O]$ are the mole fractions of SiO_2 and K_2O, respectively, $C^0_{p(SiO_2)}$ is the heat capacity of the pure SiO_2 liquid (81.4 J/mol K, Richet et al., 1984), $C^0_{p(K_2O)}$ is the heat capacity of the pure K_2O component in the melt, independent of temperature and composition, $[Q^{total}_{rings}]$ is the abundance of rings in the melt and $A(T)$ accounts for the temperature effect on $C_{p,rings}$. The heat capacity was calculated by fitting $C_{p(K_2O)}$ and $A(T)$ in the function

$$C_p = C_{p,linear} + C_{p,rings} \quad (7)$$

because no quantitative information about the abundance of three-membered rings in the melt is available, the amount of rings in the melt was approximated by the abundance of three-membered rings in the glasses (Fig. 14). However, the abundance of these rings is expected to change as a function of temperature. In fact, it is most likely the change in the abundances of these rings that is causing the excess heat capacity $C_{p,rings}$. During the fitting of the heat capacity data, the temperature effect on the abundance of the rings is reflected in the value for $A(T)$.

The heat capacities obtained with this function reproduces the measured heat capacities reasonably well, often within the uncertainty of the measured heat capacities (Fig. 15). The obtained value for $C^0_{p(K_2O)}$ is 92.3 J/mol K and the results for $A(T)$ are 0.16, 0.30 and 0.41 for 1200 K, 1500 K and 1800 K, respectively. Note that these values are sensitive to the values used for $[Q^{total}_{rings}]$, which in turn depend on the fitting function chosen in Fig. 14. Nevertheless, the value for $C^0_{p(K_2O)}$ of 92.3 J/mol K obtained here is equal within error to the value obtained by Stebbins et al. (1984), 97.0 ± 5.1 J/mol K, who fitted heat capacity data of multi-component systems, where no large fraction of three-membered rings is to be expected. As for most other properties, there is a systematic variation of the $C^0_{p(M_2O)}$ with increasing

cation size for Li < Na < K. The C_p^0 is equal to 106.8, 100.6 and 92.3 J/mol K for Li, Na (Richet and Bottinga, 1985) and K (this study), respectively. The contribution to the heat capacity that is caused by the three-membered rings increases with increasing temperature, possibly reflecting a change in the stability of three-membered rings with temperature. In K-disilicate glasses and melts, Majerus et al. (2004) observed an increase in three-membered rings with increasing temperature in the RMC models of neutron diffraction data. Based on the presence of three-membered rings in Rb- and Cs-silicate glasses, we predict a similar temperature and compositional dependence of the heat capacity.

7.3. Density

Bockris et al. (1956) and Tomlinson et al. (1958) observed deviations from additivity for the density of binary alkali and alkaline earth silicate melts, i.e. the molar volume of a melt is smaller than the weighted sum of the molar volume of the end members. They attributed these negative deviations to the accommodation of the metal cations within the structure. For the Li, Na, Mg, Ca and Sr systems, these deviations from additivity are proportional to the cube of the cation radius. However, for the K- and Ba-silicate melts, the deviations from additivity are small compared to the other cations (Tomlinson et al., 1958). It was concluded that "the accommodation of these large cations is accompanied by a structural rearrangement involving an increase in volume." For the K-silicate melts, we attribute this anomalous increase in volume (or decrease in density) to the presence of three-membered rings in the structure. For Ba-silicate glasses, Schlenz et al. (2002) observed that considerable numbers of small rings are present. This indicates that the formation of three-membered rings could also be the cause of the anomalous volumetric behavior in Ba-silicate glasses.

A decrease in density with decreasing ring size is consistent with Hobbs et al. (1998) who observed a correlation between the average ring size and the density for different crystalline and amorphous forms of silica and Stixrude and Bukowinski (1990a,b, 1991), who observed a correlation between the average ring size and density of crystalline tectosilicates. The increased abundance of three-membered rings that was observed by Raman spectroscopy in silica glass with increasing pressure (e.g. Hemley et al., 1986) seems to contradict this however.

8. CONCLUSIONS

Our data provide new constraints on the network topology, showing that three-membered rings are an abundant structural motif in K-, Rb- and Cs-silicate glasses. These rings are responsible for a temperature and non-linear compositional dependence of the heat capacity. We further suggest that these rings induce the anomalous compositional dependence of the density. Our data also shows that the viscosity (as portrayed by T_g) is related to the speciation through the entropy of mixing of the Q^n species.

These results emphasize the tight relationship between the bulk physical and thermodynamic properties and the melt structure. Hence, a model predicting these properties over a wide temperature and compositional range can only be successful if it builds on short- and medium-range structural information. The identification and quantification of the structural units in silicate melts remains a necessary step towards a better understanding of dynamic processes in magmatic systems.

ACKNOWLEDGMENTS

This project was supported by an ETH research Grant (0-20168-04) and a Swiss National Science Foundation Grant (2-7233-03) to W.H. We are grateful to the Nonmetallic Inorganic Materials (ETHZ) and N. Grundy for the use of the calorimeter. P. Ulmer and Lydia Zehnder are thanked for the XRF analysis. Part of the sample synthesis was done at the Institute of Mineralogy and Petrology (ETHZ). This manuscript was greatly enhanced by the constructive, detailed comments by the associate editor Claudia Romano, Pascal Richet and two further anonymous reviewers.

APPENDIX A. SUPPLEMENTARY DATA

Supplementary data associated with this article can be found, in the online version, at doi:10.1016/j.gca.2007.09.011.

REFERENCES

Adam G. and Gibbs J. H. (1965) On the temperature dependence of cooperative relaxation properties in glass-forming liquids. *J. Chem. Phys.* **43**(1), 139–146.

Bax A., Freeman R., Frenkiel T. A. and Levitt M. H. (1981) Assignment of carbon-13 NMR spectra via double-quantum coherence. *J. Magn. Reson. (1969)* **43**(3), 478–483.

Bax A., Freeman R. and Kempsell S. P. (1980) Natural abundance C-13–C-13 coupling observed via double-quantum coherence. *J. Am. Chem. Soc.* **102**(14), 4849–4851.

Bershtein V. A., Egorov V. M., Emel'yanov Y. A., Kelina R. P., Stepanov V. A. and Cherkas G. D. (1980) Ionic interactions between network fragments and relaxation transitions in alkali silicate glasses. *Fiz. Khim. Stekla* **6**(2), 179–180.

Bockris J. O. M., Tomlinson J. W. and White J. L. (1956) The structure of the liquid silicates: partial molar volumes and expansivities. *Trans. Faraday Soc.* **52**, 299–310.

Boesch L. P. and Moynihan C. T. (1975) Effect of thermal history on conductivity and electrical relaxation in alkali silicate glasses. *J. Non Cryst. Solids* **17**(1), 44–60.

Borisova N. V., Ushakov V. M. and Schultz M. M. (1999) Heat capacity, fictive temperature, and degrees of structural and energy ordering in vitreous potassium silicates in relation with their structure. *Glass Phys. Chem.* **25**(5), 408–413.

Brandriss M. E. and Stebbins J. F. (1988) Effects of temperature on the structure of silicate liquids: ^{29}Si NMR results. *Geochim. Cosmochim. Acta* **52**, 2659–2669.

Brawer S. A. and White W. B. (1975) Raman spectroscopic investigation of the structure of silicate glasses. I. The binary alkali silicates. *J. Chem. Phys.* **63**(6), 2421–2432.

Bourgue E. and Richet P. (2001) The effects of dissolved CO_2 on the density and viscosity of silicate melts: a preliminary study. *Earth and Planet Science Lett.* **193**(1–2), 57–68.

Casserly T. B. and Gleason K. K. (2005) Density functional theory calculation of ^{29}Si NMR chemical shifts of organosiloxanes. *J. Phys. Chem. B* **109**(28), 13605–13610.

Charpentier T., Ispas S., Profeta M., Mauri F. and Pickard C. J. (2004) First-principles calculation of ^{17}O, ^{29}Si, and ^{23}Na NMR spectra of sodium silicate crystals and glasses. *J. Phys. Chem. B* **108**, 4147–4161.

Dietzel A. and Sheybany H. A. (1948) Problèmes relatifs au remplissage des vides structuraux du verre: recherches relatives aux verres alcalino-siliceux simples. *Verres Réfractaires* **2**, 63–88.

Dupree R., Holland D., McMillan P. W. and Pettifer R. F. (1984) The structure of soda-silica glasses: a MAS NMR study. *J. Non Cryst. Solids* **68**(2–3), 399–410.

Dupree R., Holland D. and Williams D. S. (1986) The structure of binary alkali silicate glasses. *J. Non Cryst. Solids* **81**, 185–200.

Emerson J. F., Stallworth P. E. and Bray P. J. (1989) High-field ^{29}Si NMR studies of alkali silicate glasses. *J. Non Cryst. Solids* **113**, 253–259.

Ernst R. R., Bodenhausen G. and Wokaun A. (1987) *Principles of Nuclear Magnetic Resonance in One and Two Dimensions*. Clarendon Press.

Fyfe C. A., Grondey H., Feng Y. and Kokotailo G. T. (1990) Natural-abundance two-dimensional silicon-29 MAS NMR investigation of the three-dimensional bonding connectivities in the zeolite catalyst ZSM-5. *J. Am. Chem. Soc.* **112**(24), 8812–8820.

Galeener F. L. (1982a) Planar rings in glasses. *Solid State Commun.* **44**(7), 1037–1040.

Galeener F. L. (1982b) Planar rings in vitreous silica. *J. Non Cryst. Solids* **49**, 53–62.

Gedeon O., Hulinski V. and Jurek K. (2000) Microanalysis of Glass Containing Alkali Ions. *Microchim. Acta* **132**(2–4), 505–510.

Glock K., Hirsch O., Rehak P., Thomas B. and Jäger C. (1998) Novel opportunities for studying the short and medium range order of glasses by MAS NMR, ^{29}Si double quantum NMR and IR spectroscopies. *J. Non Cryst. Solids*, 113–118.

Grimmer A.-R., Mäfi M., Hähnert M., Stade H., Samoson A., Wieker W. and Lippmaa E. (1984) High-resolution solid-state ^{29}Si nuclear magnetic resonsance spectroscopic studies of binary alkali silicate glasses. *Phys. Chem. Glasses* **25**(4), 105–109.

Gurman S. J. (1990) Bond ordering in silicate glasses: a critique and a re-solution. *J. Non Cryst. Solids* **125**, 151–160.

Haouas M. and Taulelle F. (2006) Revisiting the identification of structural units in aqueous silicate solutions by two-dimensional silicon-29 INADEQUATE (vol. 110, p. 3007, 2006). *J. Phys. Chem. B* **110**(45), 22951.

Harris R. K. and Newman R. H. (1977) ^{29}Si NMR studies of aqueous silicate solutions. *J. Chem. Soc. Farraday Trans. II*, 1204–1215.

Hartmann S. R. and Hahn E. L. (1962) Nuclear double resonance in the rotating frame. *Phys. Rev.* **128**(5), 2042–2053.

Hediger S., Meier B. H. and Ernst R. R. (1995) Adiabatic passage Hartmann–Hahn cross polarization in NMR under magic angle sample spinning. *Chem. Phys. Lett.* **240**(5–6), 449–456.

Hemley R. J., Mao H. K., Bell P. M. and Mysen B. (1986) Raman spectroscopy of SiO_2 glass at high pressure. *Phys. Rev. Lett.* **57**(6), 747–750.

Hobbs L. W., Jesurum C. E., Pulim V. and Berger B. (1998) Local topology of silica networks. *Philos. Mag. Phys. Condens. Matter Struct. Defects Mech. Properties* **78**(3), 679–711.

Kubicki J. D. and Sykes D. (1993) Molecular orbital calculations of vibrations in three-membered aluminosilicate rings. *Phys. Chem. Miner.* **19**, 381–391.

Lesage A., Bardet M. and Emsley L. (1999) Through-bond carbon–carbon connectivities in disordered solids by NMR. *J. Am. Chem. Soc.* **121**(47), 10987–10993.

Machácek J. and Gedeon O. (2003) Structure of binary alkali silicate glasses—structural modifications caused by various alkali ions. *Phys. Chem. Glasses* **44**, 308–312.

Maekawa H., Maekawa T., Kawamura K. and Yokokawa T. (1991) The structural groups of alkali silicate glasses determined from ^{29}Si MAS-NMR. *J. Non Cryst. Solids* **127**, 53–64.

Majerus O., Cormier L., Calas G. and Beuneu B. (2004) A neutron diffraction study of temperature-induced structural changes in potassium disilicate glass and melt. *Chem. Geol.* **213**(1–3), 89–102.

Malfait W. J., Zakaznova-Herzog V. P. and Halter W. E. (2007) Quantitative Raman spectroscopy: high-temperature speciation of potassium silicate melts. *J. Non Cryst. Solids*. doi:10.1016/j.jnoncrysol.2007.06.031.

Masnik J. E., Kieffer J. and Bass J. D. (1993) Structural relaxations in alkali silicate systems by Brillouin light-scattering. *J. Am. Ceramic Soc.* **76**(12), 3073–3080.

Matson D. W., Sharma S. K. and Philpotts J. A. (1983) The strucure of high-silica alkali-silicate glasses. A Raman spectroscopic investigation. *J. Non Cryst. Solids* **58**, 323–352.

McMillan P. F., Grzechnik A. and Chotalla H. (1998) Structural characterization of SiO_2–$CsAlO_2$ and SiO_2–$RbAlO_2$ glasses. *J. Non Cryst. Solids* **226**(3), 239–248.

McMillan P. F., Poe B. T., Gillet P. and Reynard B. (1994) A study of SiO_2 glass and supercooled liquid to 1950 K via high-temperature Raman spectroscopy. *Geochim. Cosmochim. Acta* **58**(17), 3653–3664.

McMillan P. F., Wolf G. H. and Poe B. T. (1992) Vibrational spectroscopy of silicate liquids and glasses. *Chem. Geol.* **96**, 351–366.

Mysen B. and Richet P. (2005) *Silicate Glasses and Melts: Properties and Structure*. Elsevier.

Mysen B. O. and Frantz J. D. (1992) Raman spectroscopy of silicate melts at magmatic temperatures: Na_2O–SiO_2, K_2O–SiO_2 and Li_2O–SiO_2 binary compositions in the temperature range 25–1475 °C. *Chem. Geol.* **96**, 321–332.

Oglesby J. V. and Stebbins J. F. (2000) Si-29 CPMAS NMR investigations of silanol-group minerals and hydrous aluminosilicate glasses. *Am. Mineral.* **85**(5–6), 722–731.

Olivier L., Glock K., Thomas B. and Jäger C. (1998) Double quantum NMR and medium range order in glasses. *Glastech. Ber.* **71C**, 309.

Olivier L., Yuan X., Cormack A. N. and Jäger C. (2001) Combined ^{29}Si double quantum NMR and MD simulation studies of network connectivities of binary $Na_2O{\cdot}SiO_2$ glasses: new prospects and problems. *J. Non Cryst. Solids* **293–295**, 53–66.

Richet P. (1984) Viscosity and configurational entropy of silicate melts. *Geochim. Cosmochim. Acta* **48**, 471–483.

Richet P. and Bottinga Y. (1985) Heat capacity of aluminium-free liquid silicates. *Geochim. Cosmochim. Acta* **49**(2), 471–486.

Richet P., Bottinga Y., Denielou L., Petitet J. P. and Tequi C. (1982) Thermodynamic properties of quartz, cristobalite and amorphous SiO_2: drop calorimetry measurements between 1000 and 1800 K and a review from 0 to 2000 K. *Geochim. Cosmochim. Acta* **46**(12), 2639–2658.

Richet P., Bottinga Y. and Téqui C. (1984) Heat capacity of sodium silicate liquids. *Commun. Am. Ceramic Soc.* **67**, C6–C8.

Sasek L., Meissnerova H. and Prochazka J. (1975). *Sb. Vys. Sk. Chem. Technol. Praze, Chem. Technol. Silik.* **L6**, 95–129.

Schlenz H., Kirfel A., Schulmeister K., Wartner N., Mader W., Raberg W., Wandelt K., Oligschleger C., Bender S. and Franke R. (2002) Structure analyses of Ba-silicate glasses. *J. Non Cryst. Solids* **297**(1), 37–54.

Schmidt B. C., Riemer T., Kohn S. C., Behrens H. and Dupree R. (2000) Different water solubility mechanisms in hydrous glasses along the Qz-Ab join: evidence from NMR spectroscopy. *Geochim. Cosmochim. Acta* **64**(3), 513–526.

Shannon R. D. (1976) Revised effective ionic radii and systematic studies of interatomic distances in halides and chalcogenides. *Acta Crystallogr.* **A32**, 751–767.

Shelby J. E. (1976) Thermal-expansion of mixed-alkali silicate-glasses. *J. Appl. Phys.* **47**(10), 4489–4496.

Simakin A. G., Salova T. P., Kuchereninenko Y. V. and Zharikov v. A. (2004) Influence of cation size in the sequence Na–K–Rb on the structure of Quartz-Feldspar melts. *Petrology* **12**, 589–597.

Smith J. V. and Blackwell C. S. (1983) Nuclear magnetic resonance of silica polymorphs. *Nature* **303**, 223–225.

Stebbins J. F. (1987) Identification of multiple structural species in silicate glasses by ^{29}Si NMR. *Nature* **330**, 465–467.

Stebbins J. F. (1995) Dynamics and structure of silicate and oxide melts: nuclear magnetic resonance studies. In *Structure*, vol. 32 (eds. J. F. Stebbins, P. F. McMillan and D. B. Dingwell). Mineralogical Society of America, pp. 191–246.

Stebbins J. F., Carmichael I. S. E. and Moret L. K. (1984) Heat capacities and entropies of silicate liquids and glasses. *Contrib. Mineral. Petrol.* **86**, 131–148.

Stebbins, J. F., McMillan, P., and Dingwell, D. B. (1995) Structure, dynamics and properties of silicate melts. In *Reviews in Mineralogy* (ed. P. H. Ribbe), vol. 32.

Stixrude L. and Bukowinski M. S. T. (1990a) A novel topological compression mechanism in a covalent liquid. *Science* **250**, 541–543.

Stixrude L. and Bukowinski M. S. T. (1990b) Rings, topology and the density of tectosilicates. *Am. Mineral.* **75**, 1159–1169.

Stixrude L. and Bukowinski M. S. T. (1991) Atomic structure of SiO_2 glass and its response to pressure. *Phys. Rev. B* **44**(6), 2523.

Tomlinson J. W., Heynes M. S. R. and Bockris J. O. M. (1958) The structure of liquid silicates. *Trans. Faraday Soc.* **54**, 1822–1833.

Toplis M. J. (1998) Energy barriers to viscous flow and the prediction of the glass transition temperatures of molten silicates. *Am. Mineral.* **83**, 480–490.

Turner G. L., Smith K. A., Kirkpatrick R. J. and Oldfield E. (1986) Structure and cation effects on phosphorus-31 NMR chemical shifts adn chemical shift anisotropies of orthophosphates. *J. Magn. Reson.* **70**, 408–415.

Werthmann R. and Hoppe R. (1981) Über K_2SiO_3—das erste cyclotrisilicat eines alkalimetalls—sowie Rb_2SiO_3, Cs_2SiO_3, Rb_2GeO_3 und Cs_2GeO_3. *Rev. Chim. Minér.* **18**, 593–607.

Wicks J. D., McGreevy R. L. and Börjesson L. (1997) A network problem: modelling alkali-silicate glasses with RMC. *Phase Transit.* **61**, 195–213.

Xue X. and Kanzaki M. (2004) Dissolution mechanisms of water in depolymerized silicate melts: constraints from ^{1}H and ^{29}Si NMR spectroscopy and ab initio calculations. *Geochim. Cosmochim. Acta* **68**(24), 5027–5057.

Yasui I., Akasaka Y. and Inoue H. (1994) Re-examination of detailed structure of alkali silicate glasses based on two types of diffraction data. *J. Non Cryst. Solids* **177**, 91–96.

Associate editor: Claudia Romano